Sensors and Actuators B 238 (2017) 364–373

Contents lists available at ScienceDirect

Sensors and Actuators B: Chemical

journal homepage: www.elsevier.com/locate/snb

Xylene gas sensor based on Au-loaded $WO_3 \cdot H_2O$ nanocubes with enhanced sensing performance

Feng Li[a], Sijia Guo[a], Jingli Shen[a], Liang Shen[a], Dongming Sun[a], Bin Wang[b], Yu Chen[a,**], Shengping Ruan[a,b,*]

[a] State Key Laboratory on Integrated Optoelectronics and College of Electronic Science and Engineering, Jilin University, Changchun 130012, PR China
[b] State Key Laboratory on Applied Optics, Changchun 130023, PR China

ARTICLE INFO

Article history:
Received 22 February 2016
Received in revised form 28 June 2016
Accepted 6 July 2016
Available online 18 July 2016

Keywords:
$WO_3 \cdot H_2O$ nanocubes
Au-loaded
Xylene
Gas sensor

ABSTRACT

In this work, Au was employed as an ideal dopant to obtain enhanced sensing performance of xylene gas sensor. Firstly, the as-perpared Au-doped $WO_3 \cdot H_2O$ powder was synthesized by a facile and efficient hydrothermal method. Then various techniques including X-ray Diffraction (XRD), Scanning Electron Microscopy (SEM), Transmission Electron Microscopy (TEM) and Energy Dispersive X-ray Spectrometer (EDX) were employed to investigate the morphology, microstructure, crystalline nature and chemical compositions of the as-prepared Au-doped $WO_3 \cdot H_2O$ nanomaterials. The morphologies of the nanomaterials could be easily controlled by changing the atomic percentage (at%) of Au (0.15 at%, 0.30 at%, 0.45 at%) in the precursor solutions. And it have been attested that the 0.30 at% Au-doped $WO_3 \cdot H_2O$-based sensor realized higher gas response of 26.4–5 ppm xylene at 255 °C, faster response/recovery speed and stronger selectivity to target gas compared with the unloaded one. Furthermore, the detection limit could be as low as 200 ppb level. Hence, Au-loaded $WO_3 \cdot H_2O$ nanomaterial could be a promising material applied in xylene gas sensor.

Also, the mechanism involved in the improving xylene sensing properties of Au/$WO_3 \cdot H_2O$ was discussed.

1. Introduction

Gas sensors which constitute a very common and important class of electronic components are employed to trace specific pollutant or toxic gases reliably and expediently [1]. So gas sensors are needed for a wide range of applications including gauging the air pollution (e.g., greenhouse gas monitoring), supervising indoor air quality at a level for daily life (e.g., detection of alcohol and carbon monoxide) [2], monitoring toxic gas and gas composition in industrial production [3,4]. Including these gases, Volatile Organic Compounds (VOCs) accounts for a very large proportion. Around 200 types of VOCs, such as toluene, benzene, xylene, ethanol and acetone, are not only polluted the environment but also directly harmful to human's health [5]. Xylene, a colorless toxic gas, is inevitable and common in diverse coatings additives, various kinds of adhesives, refining of combustion gas fuel and production of synthetic fiber, rubber and plastic. Xylene is not only harmful to environment [6] but also considered to affect human health and security seriously [7] even in very low concentrations. Long-term exposure to xylene can cause health problems to human beings such as headache, dizzy, drowsiness, dermatitis and discomfort of the eyes which will end in cancer sometimes [6]. So it is weighs a lot to design a high performance xylene gas sensor. With continuous researches, plenty of high properties gas sensors in detecting CH_3CH_2OH [8,9], CH_3COCH_3 [10,11], H_2S [12,13], etc. have been obtained. However, researches on xylene detecting are not enough and the selective detection of this specific gas still remains a great challenge. This is due to the reactions between ionized oxygen species (O^{2-}, O^-, or O_2^-) and gases with similar physico-chemical properties such as xylene, toluene and benzene can induce similar chemoresistive changes [14–16] that result in increase of the resistance in p-type oxide semiconductors or decrease of the resistance in n-type oxide semiconductors. Therefore, great efforts are required to focus on the fabrication of reliable and practical xylene gas sensor.

It is generally known that bninary oxides such as SnO_2 [17,18], ZnO [19,20], Fe_2O_3 [21,22], Co_3O_4 [23,24], TiO_2 [25–27], NiO [28],

* Corresponding author at: State Key Laboratory on Integrated Optoelectronics and College of Electronic Science and Engineering, Jilin University, Changchun 130012, PR China.
** Corresponding author.
E-mail addresses: chenwy@jlu.edu.cn (Y. Chen), ruansp@jlu.edu.cn (S. Ruan).

http://dx.doi.org/10.1016/j.snb.2016.07.021
0925-4005/

etc. are typical metal oxide semiconductors (MOSs) that have been widely chosen as gas-sensing materials in recent years due to their unique electrical properties [14,15,29,30]. Sensors based on these materials show the advantages of high sensitivity, low cost, simple manufacture, fast response/recovery speed, long life, low sensitive to humidity as well as simple circuit [31]. And, these MOSs may become ideal gas sensing materials after overcoming disadvantages such as high operating temperature, poor selectivity and sharpening competitive edge by improving sensitivity and accelerating response/recovery speed [32].

Herein, we take advantage of Au-doped $WO_3 \cdot H_2O$ in this paper to detect xylene because of its special electrical properties. Various methods have been studied to synthesize this tungsten oxide compounds such as ion-exchange method [26], sol-gel [33,34], chemical vapour deposition [35,36], laser deposition [32,38,39], sputtering [33,40,41] and thermal evaporation [42,43]. However, it is common understandledge that finding out a method to resolve problems of high selectivity, fast response/recovery speed and good sensitivity at the same time is difficult in the case of gas sensors based on pure $WO_3 \cdot H_2O$. An effective route above is doping pure materials with an appropriate noble metal, which can increase the material porosity, thus increasing the specific surface area suitable for gas adsorption and consequently the sensor response [44–47]. Therefore, in this paper, the cube-like $WO_3 \cdot H_2O$ nanocrystals were successfully synthesized by a simple, effective and economical hydrothermal method at a low temperature of 120 °C for 24 h. Then Au [48–50] was introduced as a dopant to improve the properties of the sensor in this work. As it can be seen, throughout the whole process, no special equipment was employed to provide high temperature and vacuum condition which was demanded in past researches [51,52], so the device can be fabricated with low cost. Compared with the xylene gas sensor based on pure $WO_3 \cdot H_2O$, the response of Au-doped $WO_3 \cdot H_2O$ gas sensor to 5 ppm increased from 6.3 to 26.4, the response/recovery time was reduced obviously which was much faster than most reported researches [34,44,53] and selectivity was ameliorated as well. At last the possible mechanism about the improvement in the xylene sensing properties by introducing the Au dopant was discussed.

2. Experimental

2.1. Chemical reagent

In this experiment, $Na_2WO_4 \cdot 2H_2O$ (Sodium Tungstate Dihydrate) and $HAuCl_4$ (Four gold acid) were supplied by the Sinopharm Chemical Reagent Co. Ltd. $HOOC(CHOH)_2COOH$ (tartaric acid) was obtained from Beijing Chemicals Works. All the starting materials were of analytical grade and used without any further purification processes.

2.2. Synthesis process

Firstly, $WO_3 \cdot H_2O$ nanocubes were synthesized by a hydrothermal reaction [54,55] in the following sequence. In a typical process, 30 mL distilled water was used to dissolve $Na_2WO_4 \cdot 2H_2O$ (0.5 g) under magnetical stirring for 20 min at room temperature to get transparent solution. Later, 8 mL HCl aqueous solution of 3 mol/L (M) was added and the reagent was dissolved completely by stirring the solution for another 10 min. Then, different amounts of 0.01 M $HAuCl_4$ solution were added into solutions to give different doping concentration of Au. After that, 0.7 g tartaric acid was introduced. Next, the stock solution was transferred into a 50 mL Teflon-lined stainless steel autoclave to react under hydrothermal conditions at 120 °C for 24 h in sequence. Finally, the resulting product was washed several times with distilled water by the means of centrifuging to remove the ions and then dried at 60 °C in air overnight.

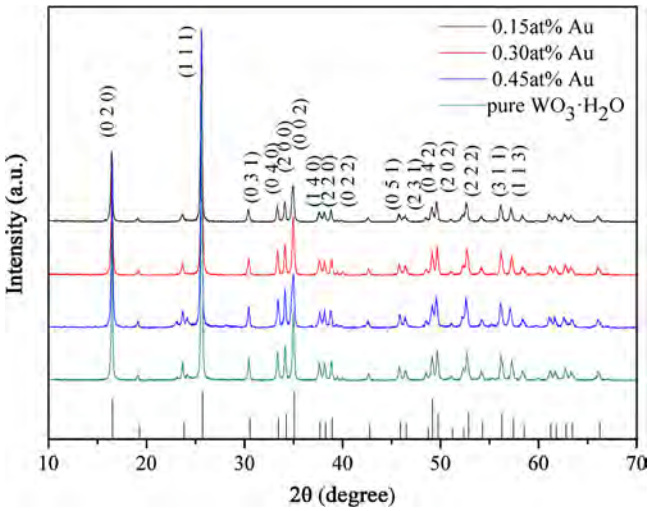

Fig. 1. XRD patterns of $WO_3 \cdot H_2O$ samples with 0 at%, 0.15 at%, 0.30 at% and 0.45 at% Au loading.

2.3. Characterization

The crystallite structures and chemical components of the samples were investigated by analyzing the wide angle X-ray Diffraction (XRD) patterns obtained with an X-ray Diffractometer (Shimadzu XRD-6000, Cu Kα radiation) and Energy Dispersive X-ray spectrogram (EDX) obtained on a JEM-ARM200F. Then a field-emission Scanning Electron Microscopy (SEM, XL30ESEM FEG) and Transmission Electron Microscope (TEM, JEOL JEM-3010) were applied to investigate the morphologies and microstructures of samples respectively.

2.4. Fabrication and measurement of sensors

The details of the sensor fabrication and the gas-sensing measurement process were similar to our previous report [37]. The as-prepared material was mixed with distilled water in a weight ratio of 4:1 evenly and then the mixture was ground in a mortar to form the corresponding paste. And the obtained paste was coated uniformly using a brush-coating method to form continuous thin film on alumina ceramic tube. On the tube, two Au electrodes were printed previously with Pt lead wires attached to both of the electrodes, and a micro-heater was inserted through the hollow centre of the ceramic tube to provide variable operating temperature of the gas sensor by tuning the heating voltage.

Next, the gas-sensing test was carried out on a CGS-8 intelligent gas sensing analysis system (Beijing Elite Tech Co. Ltd., China). And on a regular basis, the response value (S) of sensors based on n-type semiconductors is defined as $S = R_a/R_g$ for reducing gases and $S = R_g/R_a$ for oxidizing gases, where R_a is the resistance of sensors in air while R_g is the resistance in the presence of the test gas. Furthermore, the response time (τ_{res}) is defined as the duration time required for a sensor to reach 90% of the total resistance change when confront target gas (R_a to $R_a - 90\% \times (R_a - R_g)$) while the recovery time (τ_{rec}) is the time consumed to recover the resistance to 90% of the total resistance change (R_g to $R_g + 90\% \times (R_a - R_g)$) [56,57].

3. Results and discussion

3.1. Characterization

The phase and structural features of as-prepared pure, 0.15 at%, 0.30 at% and 0.45 at% Au-doped $WO_3 \cdot H_2O$ nanoparticles were analyzed by the XRD. As we can figure out in Fig. 1, inasmuch as the fairly low concentrations of the dopant that below the detection limit of XRD, four kinds of as-prepared materials showed similar curve patterns. The spectrum peaks could be indexed to (020), (111), (031), (200), (040) and (002) which suggested that all characteristic peaks were originated in $WO_3 \cdot H_2O$ nanoparticles without relating to impurities compared with No. 43-0679 of the Joint Committee on Powder Diffraction Standards card (JCPDS). Moreover, the sharp and intense diffraction peaks in patterns demonstrated the high crystallinity of the products while the broadening of the peaks was ascribed to the small size of the nanoparticles.

Fig. 2 shows a typical EDX spectrum of 0.30 at% Au/$WO_3 \cdot H_2O$ which confirmed the existence of the elements Si, O, W and Au. Besides, the Si element signal in the spectrum was attributed to such nanomaterial was pasted on the silicon wafer.

The XPS was introduced in order to illuminate the chemical state of the elements existed in the sample. 0.3 at% Au/$WO_3 \cdot H_2O$ was selected to carry out a wide scan between 0 and 1200 eV as shown in Fig. 3a. Fig. 3b shows the binding energy of W $4f_{7/2}$ and W $4f_{5/2}$ were determined to be 36.0 and 37.90 eV, respectively, which well agree with literature values for W^{6+} [58]. O 1 s XPS peaks are shown in Fig. 3c. The intense that is observed at 530.5 eV peak can be assigned to the presence of "O^{2-}" ions. And the second peak that is observed at 531.9 eV can be described as the existence of "O^{-}" ions [58]. As shown in Fig. 3d, the gold chemical state has two separate peaks located at 84.0 and 87.7 eV which are due to Au $4f_{7/2}$ and Au $4f_{5/2}$ transitions, respectively. The peaks located at 84.0 and 87.7 eV were in good agreement with the spin–orbit splitting component of Au ($4\ f_{7/2}$) level in metallic Au [59,60].

Next, in order to gain a deeper understanding of the morphology and size distribution of $WO_3 \cdot H_2O$-based nanoparticles, SEM and TEM were introduced. Fig. 4(a, c, e, g) showed the low-magnification SEM images of the pure, 0.15 at%, 0.30 at% and 0.45 at% Au-loaded $WO_3 \cdot H_2O$ precursors. From the images, it can be observed that the pure $WO_3 \cdot H_2O$ particles with small agglomerates have a rather uniform size as well as near-cube shape. The number of irregular crystal increased as expected with increase of the loading concentration. Fig. 4(b, d, f, h) showed the corresponding high magnification SEM images. Moreover, the average diameters of $WO_3 \cdot H_2O$ particles were calculated to be 87–90 nm, 290–300 nm, 308–340 nm, and 550–560 nm for the 0 at%, 0.15 at%, 0.30 at% and 0.45 at% Au-loaded $WO_3 \cdot H_2O$ precursors, respectively. Furthermore, the TEM image of the nanoparticles displayed in Fig. 5a revealed that the surfaces of 0.30 at% Au-loaded $WO_3 \cdot H_2O$ nanocrystals were clean and smooth and the dark spots immobilized on the surface uniformly and tightly were speculated to be Au NPs. Then, HRTEM result displayed in Fig. 5b confirmed this hypothesis for the lattice spacing of dark spots were measured to be about 0.236 nm corresponding to the (111) plane of Au, while the spacing between adjacent lattice planes marked was 0.347 nm, which could be indexed to the (111) plane of $WO_3 \cdot H_2O$. Its corresponding selected-area electron diffraction (SAED) pattern (Fig. 5c) shows that the Au-loaded $WO_3 \cdot H_2O$ powder was single crystalline in structure. The corresponding miller indices were accordingly indexed into the corresponding diffraction pattern, which directly related with XRD diffraction peaks (JCPDS File no. 43-0679) in Fig. 1.

In order to study the sample's surface area, the BET surface area was determined by measuring the corresponding nitrogen adsorption-desorption isotherms, which are shown in Fig. 6. Fig. 6 shows a high relative pressure that the curve exhibits a type IV isotherm with an H3 hysteresis loop according to the Brunauer-Deming-Deming-Teller (BDDT) classification. The BET surface area of the 0.3at% Au/$WO_3 \cdot H_2O$ is determined to be 17.1 m^2/g.

3.2. Gas sensing properties

In order to appraise the potential practicality and reliability of the Au-loaded $WO_3 \cdot H_2O$-based gas sensors, we carried out the investigation of fundamental gas sensing properties in the sections below. Firstly, as we know, the gas sensing performances depended on not only gas atmosphere but also operating temperature. In a more specific explanation, the highest gas sensor response would be gotten within a certain range of temperatures with operating temperature changing continuously. Fig. 7 shows the dynamic responses of gas sensors based on 0, 0.15, 0.3 and 0.45 at% Au-loaded $WO_3 \cdot H_2O$ composite nanomaterials to 5 ppm xylene to different operating temperatures. The optimum operating temperatures of all the samples were found to be 255 °C. And among three Au loaded devices, the one loaded by 0.3 at% Au showed the highest sensitivity (S = 26.4), which was 3 times larger than that of pure one (S = 6.3). Fig. 8 displayed the responses of sensors based on pure and Au-loaded $WO_3 \cdot H_2O$ nanomaterials to xylene with various concentration from 1 to 20 ppm at corresponding operating temperature. It could be easily found out that in whole concentration range, the response values of three Au-loaded gas sensors were much higher than that of the pure $WO_3 \cdot H_2O$ gas sensor.

In additional, to better understand the improvement in gas sensing properties of sensors through loading, we quantified the response and recovery rates to 1–20 ppm xylene at corresponding optimum operating temperature of the sensors based on pure and Au-loaded $WO_3 \cdot H_2O$ nanostructures by comparison. As shown in Fig. 9a and b, the response and recovery speeds for all xylene concentrations were enhanced after loading, and them were faster than a great many of recent reports as shown in Table 1. As shown in Fig. 9c, when the concentration of xylene was 1 ppm, the sensitivity of 0.3 at% Au-loaded $WO_3 \cdot H_2O$ gas sensor reached 8.1 while the pure one obtained only 2.2. With the further growth of concentrations to 20 ppm, the sensitivity of 0.3 at% Au-loaded $WO_3 \cdot H_2O$ gas sensor reached a quite high value of 36 compared with 13.2 of the pure one. It can be seen in inset Fig. 9c that a linear relationship between the response and xylene concentration was observed in range of 100–800 ppb. The detection limit of xylene for the sensor based on the 0.30 at% Au/$WO_3 \cdot H_2O$ was estimated to be approximately 200 ppb, when the criterion for gas detection was set to $R_a/R_g > 1.5$.

Finally, in order to confirm the improvement in selectivity, we carried out a response comparison of the sensors based on pure and 0.30 at% Au-loaded $WO_3 \cdot H_2O$ nanomaterials to 5 ppm different target gases. As show in Fig. 10, the responses values of the sensor based on pure $WO_3 \cdot H_2O$ to seven different kinds of target gases showed small differences that didn't obtain sufficient selectivity. In contrast, 0.30 at% Au-loaded gas sensors showed a quite significant selectivity to this specific gas owing to its higher response to xylene (26.5) in compare with the response to toluene (3.3), formaldehyde (2.47), acetone (3.87), ethanol (1.22), ammonia (1.2), benzene (1.05) nitrogen dioxide (3.47) and hydrogen sulfide (1.12).

3.3. Gas sensing mechanism

As an n-type semiconductor metal-oxide, free electrons are the main charge carriers for $WO_3 \cdot H_2O$. Hence, the performance of the $WO_3 \cdot H_2O$-based xylene sensor is on the strength of the surface interactions between adsorbed oxygen and the target gas that result in resistance variation [68,69]. The principle can be interpreted by Wolkentein's model [70] as shown in Fig. 9. Supposedly, there are serial reactions involved in the gas sensing process of

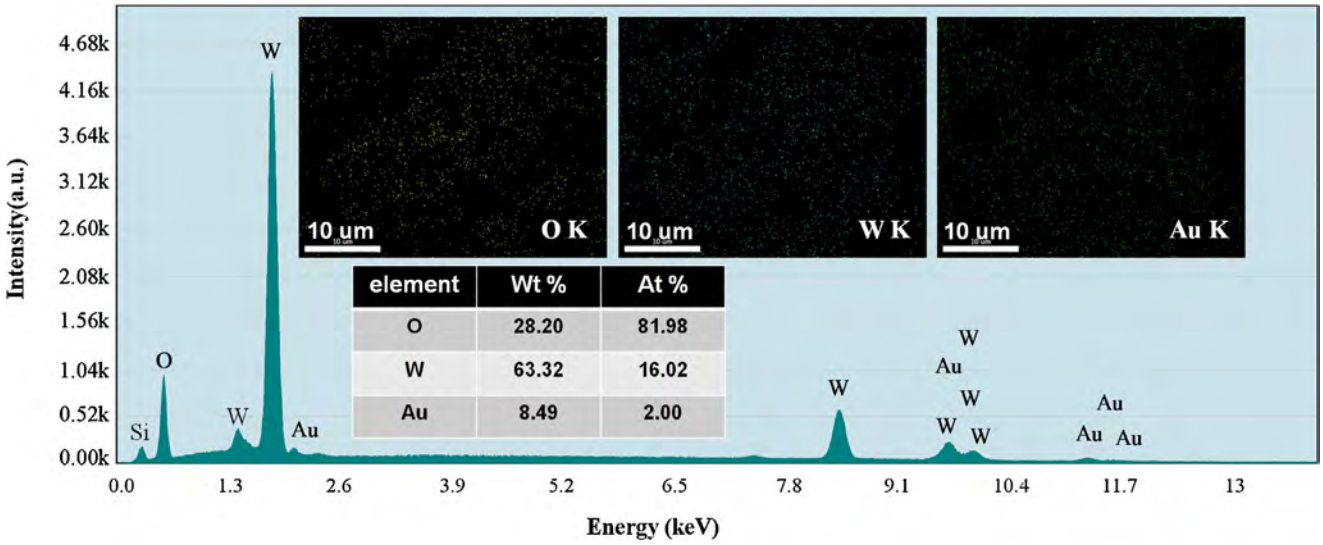

Fig. 2. EDX image of 0.30 at% Au-loaded $WO_3 \cdot H_2O$.

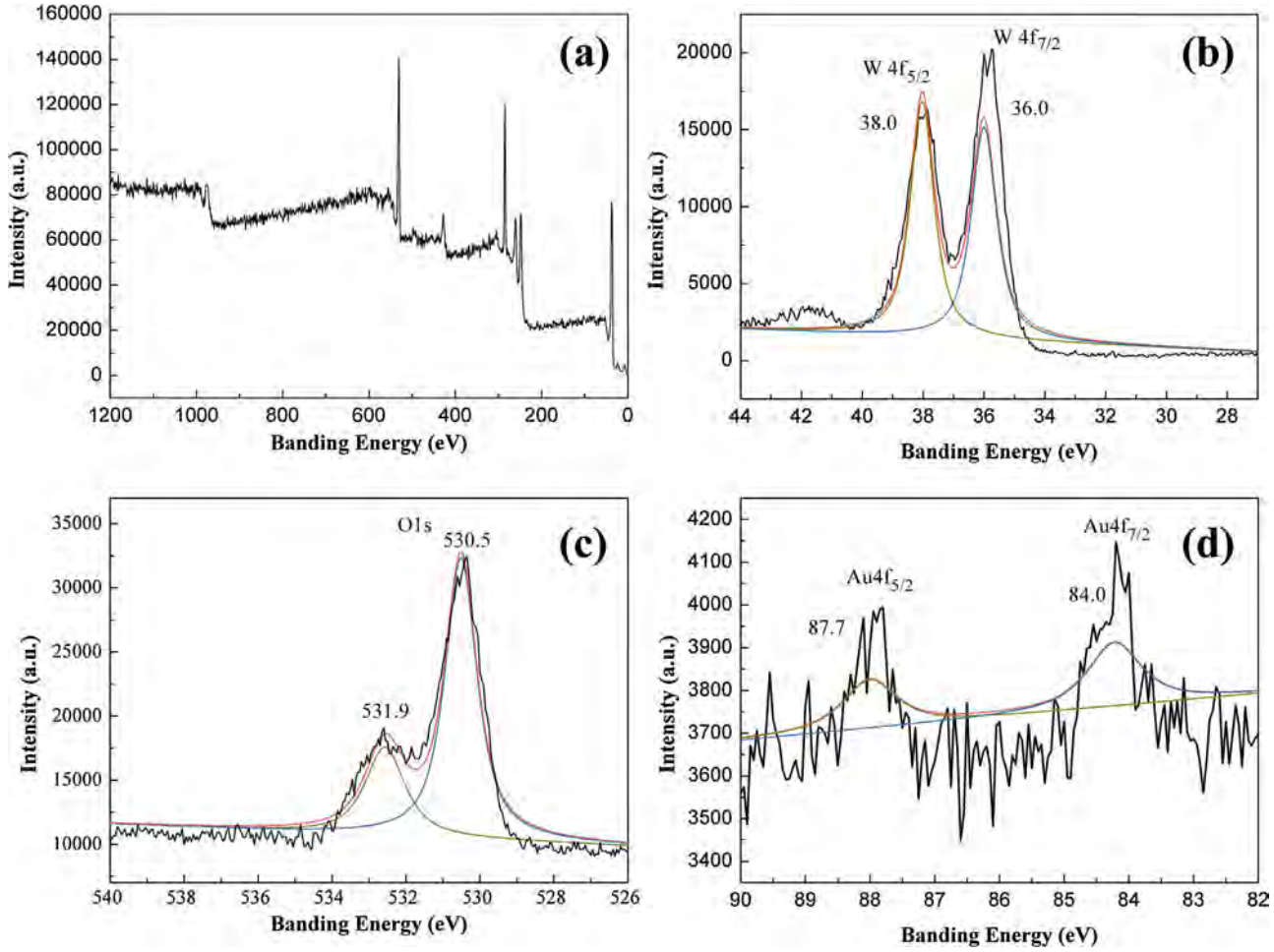

Fig. 3. (a) full survey scan spectrum of the sample; (b) W 4f; (c) O 1s; (d) Au 4f.

this kind of metal-oxide: adsorption–oxidation–desorption. When exposed to air at a proper operating temperature, $WO_3 \cdot H_2O$ particles can adsorb oxygen molecules on the surface, and the electrons from the conduction band of particles will be trapped by O_2 to form negative oxygen ions (O_2^-, O^- and O^{2-}) [71]. These reactions bring about the formation of a thick electron-depletion region that results in high resistance of the sensor consequently. The reactions can be described using the following equations [72]:

$$O_{2(gas)} \rightarrow O_{2(ads)} \quad (1)$$

$$O_{2(ads)} + e^- \rightarrow {O_2}^-{}_{(ads)} (T < 100\,^\circ C) \quad (2)$$

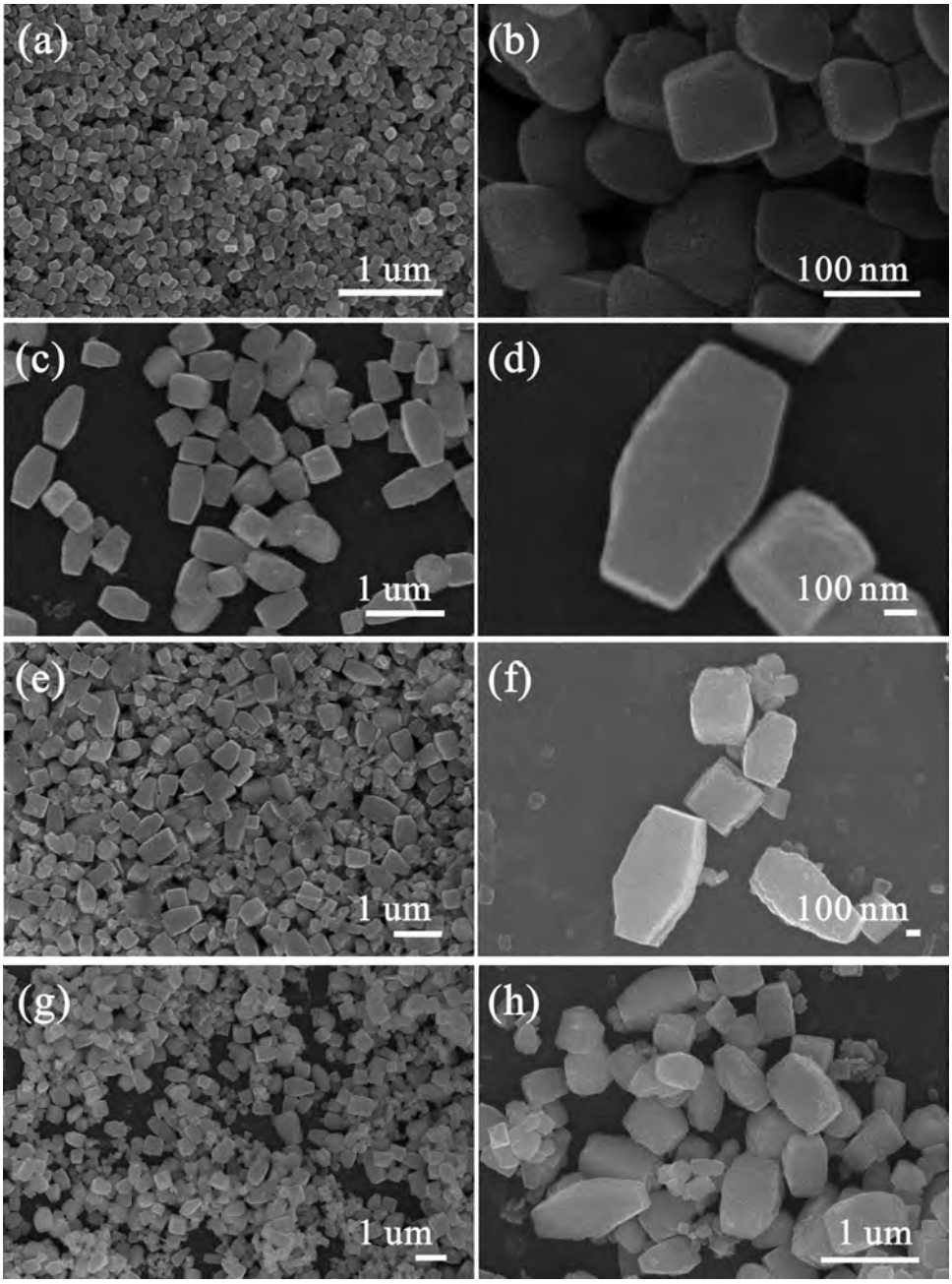

Fig. 4. SEM images of $WO_3 \cdot H_2O$ nanostructures: (a), (b) 0 at%; (c), (d) 0.15 at%; (e), (f) 0.30 at%; (g), (h) 0.45 at% Au-loaded $WO_3 \cdot H_2O$.

Table 1
Performance comparison of various gas sensors toward xylene.

Materials	Xylene (ppm)	Response time	Recovery time
our experiment	10	1s	1s
Ni doped TiO_2 bowl-like submicron particles [61]	100	9 s	1.2 s
α-MoO_3/α-Fe_2O_3 heterostructure [62]	100	87 s	190 s
mesoporous α-Fe_2O_3 nanostructures[63]	1000	1 s	13 s
double-layered thin film and Ni-deposited porous alumina [64]	10	20 s	300 s
α-MoO3 nanobelts [65]	100	7 s	87 s
aryl-bridged polysilsesquioxane thin films coupled to gold nanoparticles [66]	30	6–9 min	26–30 min
Co_3O_4 Nanofibers [67]	100	15 s	22 s

$$O_2{}^-{}_{(ads)} + e^- \rightarrow 2O^-{}_{(ads)} (100\,^\circ C < T < 300\,^\circ C) \quad (3)$$

$$O^-{}_{(ads)} + e^- \rightarrow O^{2-}{}_{(ads)} (T > 300\,^\circ C) \quad (4)$$

When $WO_3 \cdot H_2O$-based sensors are exposed to the target gas, xylene molecules will be adsorbed on the surface of the particles and oxidized by oxygen species ($O_2{}^-$, O^- and O^{2-}) to form CO_2 and H_2O. Thus, electrons are released back to the conduction band of

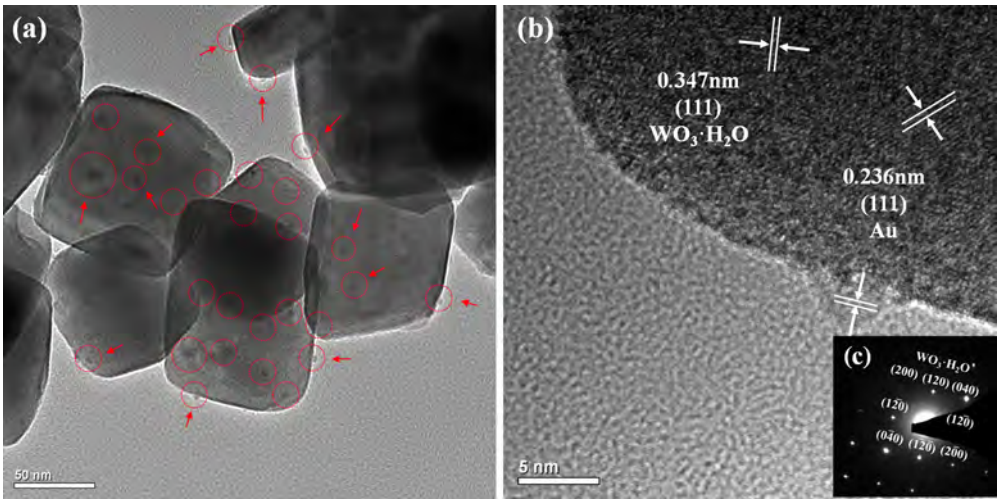

Fig. 5. (a) Typical TEM image of 0.30 at% Au-loaded $WO_3 \cdot H_2O$; (b) HRTEM image taken from (a); (c) the corresponding SAED pattern.

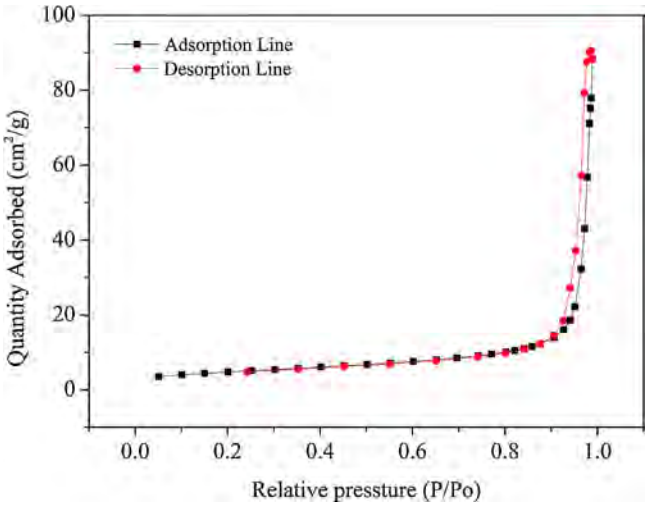

Fig. 6. Typical N_2 adsorption-desorption isotherms of 0.30 at% Au-doped $WO_3 \cdot H_2O$.

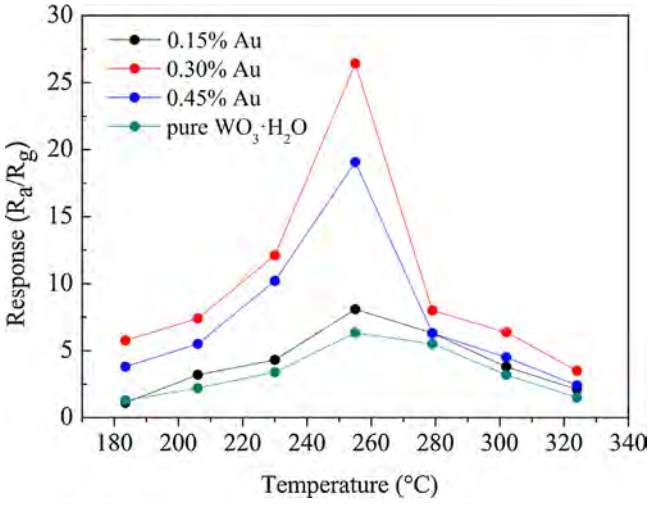

Fig. 7. Optimum working temperature of the sensors to xylene gas at a concentration of 5 ppm.

$WO_3 \cdot H_2O$ which leads to a great increase in the density of charge carriers. Then the electron depletion layer narrows down, after that, the resistance of $WO_3 \cdot H_2O$ reduces as a consequence. Here are some possible equations of methyl groups because the reactions of xylene are complex [42,73]:

$$C_6H_4CH_3CH_3(g) \rightarrow (C_6H_4CH_3CH_3)_{ads} \quad (5)$$

$$(C_6H_4CH_3CH_3)_{ads} + 2O^-_{(ads)} \rightarrow (C_6H_4CH_3CHO) + H_2O + 2e^- \quad (6)$$

$$(C_6H_4CH_3CHO) + xO^-_{(ads)} \rightarrow CO_x + H_2O(g) + xe^- \quad (7)$$

Furthermore, as the model mentioned above, when the operating temperature increases, higher response will be achieved because of the activation of negative oxygen ions and adsorbed molecular oxygen. However, if temperature continues to increase and exceeds the certain optimum temperature, the adsorption of exothermic gas becomes difficult and gas molecules begin to desorb in large quantities as well that leads to a reducing in sensor response [74,75]. Thus, the optimum temperature is a balance of activation and desorption.

According to the analysis of the possible gas sensing mechanism, the first reason for the enhancement in gas sensing performance of Au loaded $WO_3 \cdot H_2O$-based xylene gas sensor is that Au reacts as a catalyst [76,77]. When the methyl groups of xylene connected to the benzene ring are oxidized, they are dehydrogenated by the

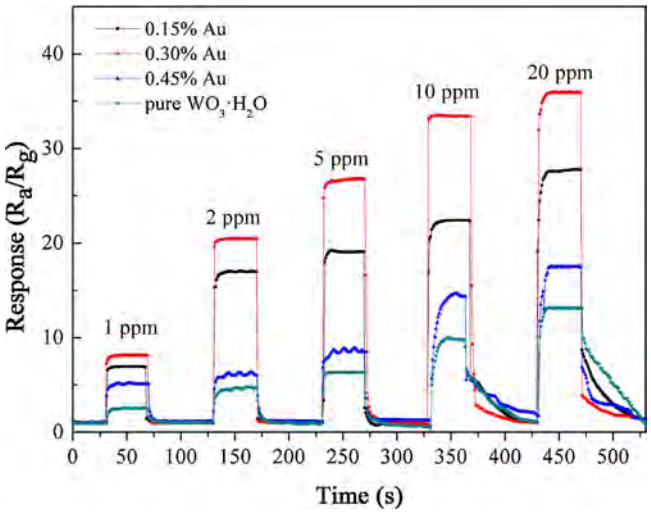

Fig. 8. Gas-sensing transients to 1–20 ppm xylene operated at optimal operating temperature.

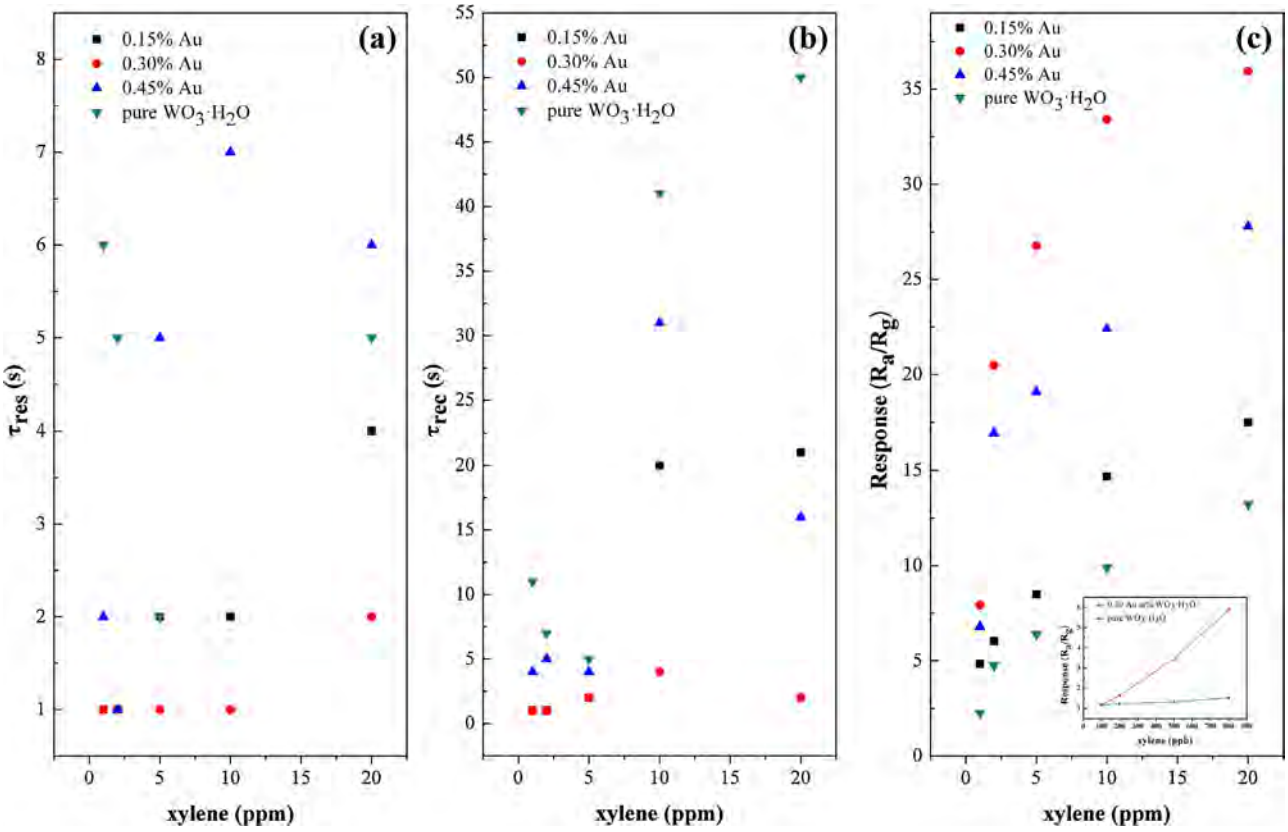

Fig. 9. (a) Response time and (b) recovery time of $WO_3 \cdot H_2O$ samples to 1–20 ppm xylene, (c) responses of pure and 0.30 at% Au-loaded $WO_3 \cdot H_2O$ versus xylene concentrations (1–20 ppm).

oxygen ions attached to the surface of the materials first. The activation of Au can lower enthalpy change of dehydrogenation of xylene, which can lead to higher response. Therefore, the activity energy decreases while the sensing reaction is accelerated (Eq. (6)) leading an enhanced performance.

Secondly, the model of spill-over effect is introduced to explain the effect of noble metal additives on metal oxide-based gas sensors [78]. Separate metallic nanoparticles on the surface of the supporting metal oxide play an important role to enrich the surface or the interface, which leads to the enhancement of the chemical activity of xylene and oxygen molecules to make them easier to be absorbed and reacted with on the surface. The responsible sensing reaction, such as the reaction of xylene with pre-adsorbed oxygen ions, takes place at the surface of the host metal oxide which determines the release of electrons to the conduction band of the semiconducting metal oxide.

Thirdly, the enhanced xylene sensing properties may be attributed to Schottky junction between Au and $WO_3 \cdot H_2O$. When Au and $WO_3 \cdot H_2O$ contact with each other, they would joint together to form Schottky junction at the interface due to different band gaps and work functions [79,80]. Because the sensing reactions happen on the surface of nanomaterials, this Schottky junction will remarkably enhance the gas sensing performance as expected [81]. As illustrated in Fig. 9b, when exposed to xylene ambient, a thicker electron depletion layer will be obtained on the surface region and interfaces of Au and $WO_3 \cdot H_2O$ compared with the pure one. As a result, the target gases are allowed to react with more adsorbed oxygen ions. Thus, more trapped electrons can return to the conduction band of the $WO_3 \cdot H_2O$ leading to larger change in resistance which means a higher response. Hence, we deduce that Au may be the reason for enhanced performance to xylene (Fig. 11).

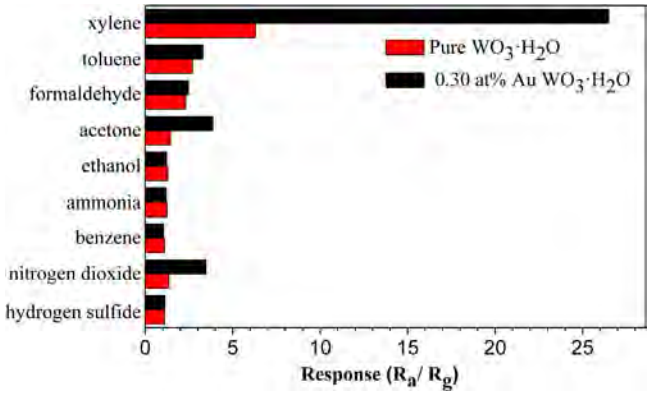

Fig. 10. Responses of the pure and 0.30 at% Au-loaded $WO_3 \cdot H_2O$ exposed to 5 ppm different target gases at their optimal operating temperature.

Besides, we suppose that quantum-well effect plays an important role in gas sensing process. As shown in Fig. 12b, when Au was loaded onto the surface of $WO_3 \cdot H_2O$, they would joint together to form band bending at the interface due to the different work functions. The nanoscale multilayered sensing material composed of Au and $WO_3 \cdot H_2O$ which two alternating nanoscale layers used in this paper developed multiple band bending which could be seen as quantum well as shown in Fig. 12a. When the material is exposed to atmosphere, electrons are constrained in quantum-wells, which results in decrease of the number of free carriers and increase of resistance. When the material is exposed to xylene, the target gas would react with oxygen ions absorbed on the surface of gas sensing material and a great number of free electrons are released. As a result, the band bending degree and the potential barriers are

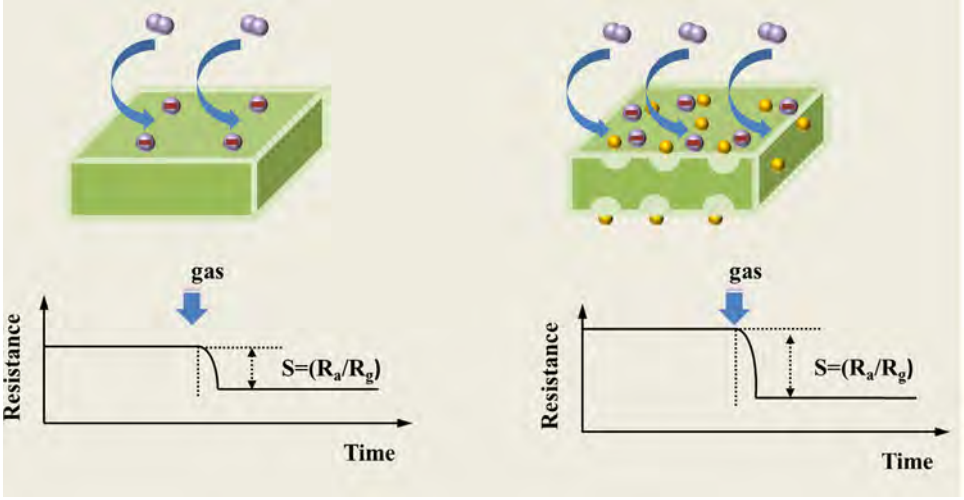

Fig. 11. Schematic diagrams of the sensing mechanism of (a) pure; (b) Au-loaded $WO_3 \cdot H_2O$.

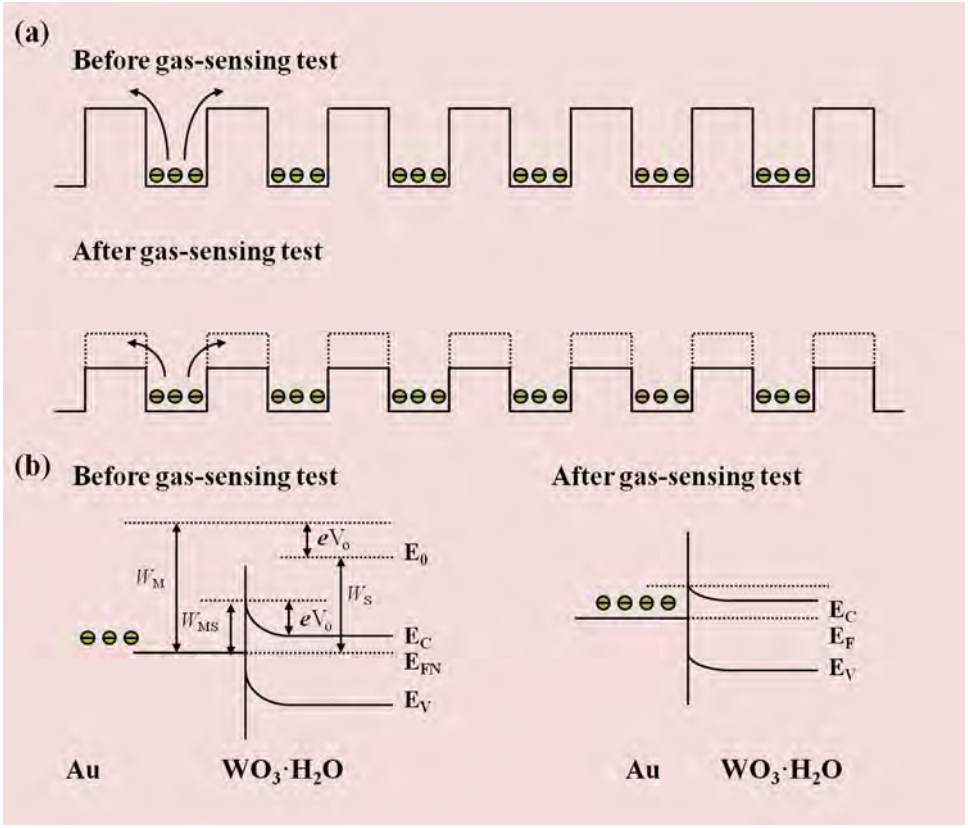

Fig. 12. (a) Schematic diagrams of quantum well changing of Au-loaded WO3·H2O before and after gas-sensing test; (b) changing of work function, band energy, and potential barrier before and after gas-sensing test.

reduced, the depth of field of quantum well becomes shallow, so the constrained electrons could get over the potential barrier easily, which leads to the increase of the number of free carriers and decrease of resistance of material. Furthermore, in two dimensional quantum well, as the migration of electrons was constrained in one-dimensional, the moving speed of electrons increases obviously leading to an accelerated response rate. We know that VOCs gases have carbon hydrogen bonds and Au nanoparticles have catalytic effect for dehydrogenation reaction [76,77]. The plane structure and the π-conjugate system of the benzene ring in xylene makes it more easily react with oxygen ions absorbed in the surface of Au-loaded $WO_3 \cdot H_2O$ than other VOCs gas. Hence, Au-loaded $WO_3 \cdot H_2O$ can sense in selective to VOCs category especially to xylene.

4. Conclusions

In summary, we demonstrated a facile and efficient hydrothermal method in this paper to synthesize Au-loaded $WO_3 \cdot H_2O$ nanomaterials at the temperature as low as 120 °C without the assistance of any expensive equipment to provide high temperature and vacuum condition. Compared with the pure $WO_3 \cdot H_2O$ gas sensor, it can be confirmed that the 0.3 at% Au-loaded WO_3

gas sensors exhibit enhanced xylene sensing properties, including higher response (26.4–5 ppm xylene), faster response/recovery characteristics and better selectivity. At the same time, 0.3 at% Au-loaded WO_3 gas sensors exhibited low optimum temperature and low detection limit. The excellent gas sensing performance of Au-loaded $WO_3{\cdot}H_2O$ sensor might be attributed to the synergistic effects of catalysis of Au nanoparticles and the presence of Au/$WO_3{\cdot}H_2O$ Schottky junction. The results certified that Au-loaded $WO_3{\cdot}H_2O$ gas sensor is a promising candidate for a good performance xylene sensor.

Acknowledgements

The authors are grateful to National Natural Science Foundation of China (Grant No.61274068, 11574110), Project of Science and Technology Plan of Changchun City (Grant No. 14KG020, 14KG019), Opened Fund of the State Key Laboratory on Integrated Optoelectronics No. IOSKL2013KF10) and Opened Fund of the State Key Laboratory on Applied Optics.

References

[1] X. Liu, S. Cheng, H. Liu, S. Hu, D. Zhang, H. Ning, A survey on gas sensing technology, Sensors 12 (2012) 9635–9665.
[2] M.T. Ke, M.T. Lee, C.Y. Lee, L.M. Fu, A MEMS-based benzene gas sensor with a self-heating WO_3 sensing layer, Sensors 9 (2009) 2895–2906.
[3] D. Chen, S. Lei, Y. Chen, A single polyaniline nanofiber field effect transistor and its gas sensing mechanisms, Sensors 11 (2011) 6509–6516.
[4] N. Tamaekong, C. Liewhiran, A. Wisitsoraat, S. Phanichphant, Flame-spray-made undoped zinc oxide films for gas sensing applications, Sensors 10 (2010) 7863–7873.
[5] K. Inyawilert, A. Wisitsora-At, A. Tuantranont, P. Singjai, S. Phanichphant, C. Liewhiran, Ultra-rapid VOCs sensors based on sparked-In_2O_3 sensing films, Sens. Actuators B 192 (2014) 745–754.
[6] T. Akiyama, Y. Ishikawa, K. Hara, Xylene sensor using double-layered thin film and Ni-deposited porous alumina, Sens. Actuators B-Chem. 181 (2013) 348–352.
[7] H.J. Kim, J.W. Yoon, K.I. Choi, H.W. Jang, A. Umar, J.H. Lee, Ultraselective and sensitive detection of xylene and toluene for monitoring indoor air pollution using Cr-doped NiO hierarchical nanostructures, Nanoscale 5 (2013) 7066–7073.
[8] D. Ju, H. Xu, J. Zhang, J. Guo, B. Cao, Direct hydrothermal growth of ZnO nanosheets on electrode for ethanol sensing, Sens. Actuators B-Chem. 201 (2014) 444–451.
[9] G. Chen, S. Ji, H. Li, X. Kang, S. Chang, Y. Wang, G. Yu, J. Lu, J. Claverie, Y. Sang, H. Liu, High-energy faceted SnO_2-coated TiO_2 nanobelt heterostructure for near-ambient temperature-responsive ethanol sensor, ACS Appl. Mater. Interfaces 7 (2015) 24950–24956.
[10] T. Xiao, X.-Y. Wang, Z.-H. Zhao, L. Li, L. Zhang, H.-C. Yao, J.-S. Wang, Z.-J. Li, Highly sensitive and selective acetone sensor based on C-doped WO_3 for potential diagnosis of diabetes mellitus, Sens. Actuators B-Chem. 199 (2014) 210–219.
[11] S.B. Upadhyay, R.K. Mishra, P.P. Sahay, Enhanced acetone response in co-precipitated WO_3 nanostructures upon indium doping, Sens. Actuators B-Chem. 209 (2015) 368–376.
[12] S.J. Choi, I. Lee, B.H. Jang, D.Y. Youn, W.H. Ryu, C.O. Park, I.D. Kim, Selective diagnosis of diabetes using Pt-functionalized WO_3 hemitube networks as a sensing layer of acetone in exhaled breath, Anal. Chem. 85 (2013) 1792–1796.
[13] W. Zang, Y. Nie, D. Zhu, P. Deng, L. Xing, X. Xue, Core–shell In_2O_3/ZnO nanoarray nanogenerator as a self-powered active gas sensor with high H_2S sensitivity and selectivity at room temperature, J. Phys. Chem. 118 (2014) 9209–9216.
[14] Y. Liu, J. Dong, P.J. Hesketh, M. Liu, Synthesis and gas sensing properties of ZnO single crystal flakes, J. Mater. Chem. 15 (2005) 2316.
[15] F. Sun, W. Cai, Y. Li, L. Jia, F. Lu, Direct growth of mono- and multilayer nanostructured porous films on curved surfaces and their application as gas sensors, Adv. Mater. 17 (2005) 2872–2877.
[16] X. Gou, G. Wang, J. Yang, J. Park, D. Wexler, Chemical synthesis, characterisation and gas sensing performance of copper oxide nanoribbons, J. Mater. Chem 18 (2008) 965.
[17] K.-M. Li, Y.-J. Li, M.-Y. Lu, C.-I. Kuo, L.-J. Chen, Direct conversion of single-layer SnO nanoplates to multi-layer SnO_2 nanoplates with enhanced ethanol sensing properties, Adv. Funct. Mater. 19 (2009) 2453–2456.
[18] J. Huang, X. Xu, C. Gu, W. Wang, B. Geng, Y. Sun, J. Liu, Effective VOCs gas sensor based on porous SnO_2 microcubes prepared via spontaneous phase segregation, Sens. Actuators B-Chem. 173 (2012) 599–606.
[19] Z. Jing, J. Zhan, Fabrication and gas-sensing properties of porous ZnO nanoplates, Adv. Mater. 20 (2008) 4547–4551.
[20] L. Wang, Z. Lou, T. Fei, T. Zhang, Zinc oxide core?shell hollow microspheres with multi-shelled architecture for gas sensor applications, J. Mater. Chem. 21 (2011) 19331.
[21] M. Hulko, I. Hospach, N. Krasteva, G. Nelles, Cytochrome c biosensor—a model for gas sensing, Sensors 11 (2011) 5968–5980.
[22] H.-J. Kim, K.-I. Choi, A. Pan, I.-D. Kim, H.-R. Kim, K.-M. Kim, C.W. Na, G. Cao, J.-H. Lee, Template-free solvothermal synthesis of hollow hematite spheres and their applications in gas sensors and Li-ion batteries, J. Mater. Chem. 21 (2011) 6549.
[23] H.-M. Jeong, H.-J. Kim, P. Rai, J.-W. Yoon, J.-H. Lee, Cr-doped Co_3O_4 nanorods as chemiresistor for ultraselective monitoring of methyl benzene, Sens. Actuators B-Chem. 201 (2014) 482–489.
[24] L.-L. Xing, Z.-H. Chen, X.-Y. Xue, Controllable synthesis Co_3O_4 nanorods and nanobelts and their excellent lithium storage performance, Solid State Sci. 32 (2014) 88–93.
[25] W.C. Tian, Y.H. Ho, C.H. Chen, C.Y. Kuo, Sensing performance of precisely ordered TiO_2 nanowire gas sensors fabricated by electron-beam lithography, Sensors 13 (2013) 865–874.
[26] Z. Lou, F. Li, J. Deng, L. Wang, T. Zhang, Branch-like hierarchical heterostructure (alpha-Fe_2O_3/TiO_2): a novel sensing material for trimethylamine gas sensor, ACS Appl. Mater. Interfaces 5 (2013) 12310–12316.
[27] M.-H. Seo, M. Yuasa, T. Kida, J.-S. Huh, N. Yamazoe, K. Shimanoe, Microstructure control of TiO_2 nanotubular films for improved VOC sensing, Sens. Actuators B-Chem. 154 (2011) 251–256.
[28] G. Zhu, C. Xi, H. Xu, D. Zheng, Y. Liu, X. Xu, X. Shen, Hierarchical NiO hollow microspheres assembled from nanosheet-stacked nanoparticles and their application in a gas sensor, RSC Adv. 2 (2012) 4236.
[29] N.M. Vuong, D. Kim, H. Kim, Electrochromic properties of porous WO_3–TiO_2 core–shell nanowires, J. Mater. Chem. C 1 (2013) 3399.
[30] P.J. Wojcik, A.S. Cruz, L. Santos, L. Pereira, R. Martins, E. Fortunato, Microstructure control of dual-phase inkjet-printed a—WO_3/TiO_2/WOX films for high-performance electrochromic applications, J. Mater. Chem. 22 (2012) 13268.
[31] R.D. Kornbluh, R. Pelrine, Q. Pei, R. Heydt, S. Stanford, S. Oh, J. Eckerle, Electroelastomers: applications of dielectric elastomer transducers for actuation, generation, and smart structures, SPIE's 9th Annual International Symposium on Smart Structures and Materials, Int. Soc. Opt. and Photonics (2002) 254–270.
[32] Z. Liu, T. Fan, D. Zhang, X. Gong, J. Xu, Hierarchically porous ZnO with high sensitivity and selectivity to H_2S derived from biotemplates, Sens. Actuators B-Chem. 136 (2009) 499–509.
[33] L.G. Teoh, Y.M. Hon, J. Shieh, W.H. Lai, M.H. Hon, Sensitivity properties of a novel NO_2 gas sensor based on mesoporous WO_3 thin film, Sens. Actuators B-Chem. 96 (2003) 219–225.
[34] A. Hazra, K. Dutta, B. Bhowmik, P. Bhattacharyya, Highly repeatable low-ppm ethanol sensing characteristics of p-TiO_2-based resistive devices, IEEE Sens. J. 15 (2015) 408–416.
[35] N. Shankar, M.-F. Yu, S.P. Vanka, N.G. Glumac, Synthesis of tungsten oxide (WO_3) nanorods using carbon nanotubes as templates by hot filament chemical vapor deposition, Mater. Lett. 60 (2006) 771–774.
[36] A.H. Mahan, P.A. Parilla, K.M. Jones, A.C. Dillon, Hot-wire chemical vapor deposition of crystalline tungsten oxide nanoparticles at high density, Chem. Phys. Lett. 413 (2005) 88–94.
[37] F. Li, Y. Li, F. Jing, J. Zhou, Y. Chen, D. Sun, S. Ruan, Low-temperature synthesis of WO_3 nanolamella and their sensing properties for xylene, RSC Adv. 5 (2015) 85598–85605.
[38] F. Di Fonzo, A. Bailini, V. Russo, A. Baserga, D. Cattaneo, M.G. Beghi, P.M. Ossi, C.S. Casari, A. Li Bassi, C.E. Bottani, Synthesis and characterization of tungsten and tungsten oxide nanostructured films, Catal. Today 116 (2006) 69–73.
[39] K.J. Lethy, D. Beena, R. Vinod Kumar, V.P. Mahadevan Pillai, V. Ganesan, V. Sathe, Structural, optical and morphological studies on laser ablated nanostructured WO_3 thin films, Appl. Surf. Sci. 254 (2008) 2369–2376.
[40] M.U. Qadri, A.F. Diaz, M. Cittadini, A. Martucci, M.C. Pujol, J. Ferre-Borrull, E. Llobet, M. Aguilo, F. Diaz, Effect of Pt nanoparticles on the optical gas sensing properties of WO_3 thin films, Sensors 14 (2014) 11427–11443.
[41] H. Zheng, A.Z. Sadek, K. Latham, K. Kalantar-Zadeh, Nanoporous WO_3 from anodized RF sputtered tungsten thin films, Electrochem. Commun. 11 (2009) 768–771.
[42] D.Z. Guo, K. Yu-Zhang, A. Gloter, G.M. Zhang, Z.Q. Xue, Synthesis and characterization of tungsten oxide nanorods, J. Mater. Res. 19 (2011) 3665–3670.
[43] A. Ponzoni, E. Comini, M. Ferroni, G. Sberveglieri, Nanostructured WO_3 deposited by modified thermal evaporation for gas-sensing applications, Thin Solid Films 490 (2005) 81–85.
[44] S.D. Shinde, G.E. Patil, D.D. Kajale, V.B. Gaikwad, G.H. Jain, Synthesis of ZnO nanorods by spray pyrolysis for H_2S gas sensor, J. Alloy Compd. 528 (2012) 109–114.
[45] D. Kohl, The role of noble metals in the chemistry of solid-state gas sensors, Sens. Actuators B-Chem. 1 (1990) 158–165.
[46] T. Samerjai, N. Tamaekong, C. Liewhiran, A. Wisitsoraat, S. Phanichphant, NO_2 gas sensing of flame-made Pt-loaded WO_3 thick films, J. Solid State Chem. 214 (2014) 47–52.
[47] S. Singkammo, A. Wisitsoraat, C. Sriprachuabwong, A. Tuantranont, S. Phanichphant, C. Liewhiran, Electrolytically exfoliated graphene-loaded

flame-made Ni-doped SnO_2 composite film for acetone sensing, ACS Appl. Mater. Interfaces 7 (2015) 3077–3092.
[48] X. Yang, V. Salles, Y.V. Kaneti, M. Liu, M. Maillard, C. Journet, X. Jiang, A. Brioude, Fabrication of highly sensitive gas sensor based on Au functionalized WO_3 composite nanofibers by electrospinning, Sens. Actuators B-Chem. 220 (2015) 1112–1119.
[49] H. Xia, Y. Wang, F. Kong, S. Wang, B. Zhu, X. Guo, J. Zhang, Y. Wang, S. Wu, Au-doped WO_3-based sensor for NO_2 detection at low operating temperature, Sens. Actuators B-Chem. 134 (2008) 133–139.
[50] Z. Hosseini, A. Mortezaali, S. Fardindoost, Sensitive and selective room temperature H_2S gas sensor based on Au sensitized vertical ZnO nanorods with flower-like structures, J. Alloy Compd. 628 (2015) 222–229.
[51] A. Arfaoui, S. Touihri, A. Mhamdi, A. Labidi, T. Manoubi, Structural morphological, gas sensing and photocatalytic characterization of MoO_3 and WO_3 thin films prepared by the thermal vacuum evaporation technique, Appl. Surf. Sci. 357 (2015) 1089–1096.
[52] M. Afshar, E.M. Preiß, T. Sauerwald, M. Rodner, D. Feili, M. Straub, K. König, A. Schütze, H. Seidel, Indium-tin-oxide single-nanowire gas sensor fabricated via laser writing and subsequent etching, Sens. Actuators B-Chem. 215 (2015) 525–535.
[53] M.-T. Ke, M.-T. Lee, C.-Y. Lee, L.-M. Fu, A MEMS-based benzene gas sensor with a self-heating WO_3 sensing layer, Sensors 9 (2009) 2895–2906.
[54] V.B. Patil, P.V. Adhyapak, S.S. Suryavanshi, I.S. Mulla, Oxalic acid induced hydrothermal synthesis of single crystalline tungsten oxide nanorods, J. Alloy Compd. 590 (2014) 283–288.
[55] W. Zeng, Y. Li, B. Miao, K. Pan, Hydrothermal synthesis and gas sensing properties of $WO_3 \cdot H_2O$ with different morphologies, Physica E 56 (2014) 183–188.
[56] D. Chen, L. Yin, L. Ge, B. Fan, R. Zhang, J. Sun, G. Shao, Low-temperature and highly selective NO-sensing performance of WO_3 nanoplates decorated with silver nanoparticles, Sens. Actuators B-Chem. 185 (2013) 445–455.
[57] L. Yin, D. Chen, M. Hu, H. Shi, D. Yang, B. Fan, G. Shao, R. Zhang, G. Shao, Microwave-assisted growth of In_2O_3 nanoparticles on WO_3 nanoplates to improve H_2S-sensing performance, J. Mater. Chem. A 2 (2014) 18867–18874.
[58] J.C. Dupin, D. Gonbeau, P. Vinatier, A. Levasseur, Systematic XPS studies of metal oxides, hydroxides and peroxides, Phys. Chem. Chem. Phys. 2 (2000) 1319–1324.
[59] P. Sangpour, O. Akhavan, A.Z. Moshfegh, M. Roozbehi, Formation of gold nanoparticles in heat-treated reactive co-sputtered Au-SiO_2 thin films, Appl. Surf. Sci. 254 (2007) 286–290.
[60] T. Ohgi, H.Y. Sheng, Z.C. Dong, H. Nejoh, D. Fujita, Charging effects in gold nanoclusters grown on octanedithiol layers, Appl. Phys. Lett. 79 (2001) 2453–2455.
[61] L. Zhu, D. Zhang, Y. Wang, C. Feng, J. Zhou, C. Liu, et al., Xylene gas sensor based on Ni doped TiO_2 bowl-like submicron particles with enhanced sensing performance, RSC Adv. 5 (2015) 28105–28110.
[62] D. Jiang, W. Wei, F. Li, Y. Li, C. Liu, D. Sun, et al., Xylene gas sensor based on α-MoO_3/α-Fe_2O_3 heterostructure with high response and low operating temperature, RSC Adv. 5 (2015) 39442–39448.
[63] Y. Li, Y. Cao, D. Jia, Y. Wang, J. Xie, Solid-state chemical synthesis of mesoporous α-Fe_2O_3 nanostructures with enhanced xylene-sensing properties, Sens. Actuators B 198 (2014) 360–365.
[64] T. Akiyama, Y. Ishikawa, K. Hara, Xylene sensor using double-layered thin film and Ni-deposited porous alumina, Sens. Actuators B 181 (2013) 348–352.
[65] D. Jiang, Y. Wang, W. Wei, F. Li, Y. Li, L. Zhu, et al., Xylene sensor based on α-MoO_3 nanobelts with fast response and low operating temperature, RSC Adv. 5 (2015) 18655–18659.
[66] L. Brigo, M. Cittadini, L. Artiglia, G.A. Rizzi, G. Granozzi, M. Guglielmi, et al., Xylene sensing properties of aryl-bridged polysilsesquioxane thin films coupled to gold nanoparticles, J. Mater. Chem. C 1 (2013) 4252–4260.
[67] F. Qu, C. Feng, C. Li, W. Li, S. Wen, S. Ruan, et al., Preparation and xylene©\sensing properties of Co_3O_4 nanofibers, Int. J. Appl. Ceram. Technol. 11 (2014) 619–625.
[68] D.E. Williams, Semiconducting oxides as gas-sensitive resistors, Sens. Actuators B-Chem. 57 (1999) 1–16.
[69] N. Barsan, U. Weimar, Conduction model of metal oxide gas sensors, J. Electroceram. 7 (2001) 143–167.
[70] X. Liu, N. Chen, X. Xing, Y. Li, X. Xiao, Y. Wang, I. Djerdj, A high-performance n-butanol gas sensor based on ZnO nanoparticles synthesized by a low-temperature solvothermal route, RSC Adv. 5 (2015) 54372–54378.
[71] X. An, C.Y. Jimmy, Y. Wang, Y. Hu, X. Yu, G. Zhang, WO_3 nanorods/graphene nanocomposites for high-efficiency visible-light-driven photocatalysis and NO_2 gas sensing, J. Mater. Chem. 22 (2012) 8525–8531.
[72] N. Han, H. Liu, X. Wu, D. Li, L. Chai, Y. Chen, Pure and Sn-, Ga-and Mn-doped ZnO gas sensors working at different temperatures for formaldehyde, humidity, NH_3, toluene and CO, Appl. Phys. A 104 (2011) 627–633.
[73] L. Yin, D. Chen, M. Feng, L. Ge, D. Yang, Z. Song, B. Fan, R. Zhang, G. Shao, Hierarchical Fe_2O_3@WO_3 nanostructures with ultrahigh specific surface areas: microwave-assisted synthesis and enhanced H_2S-sensing performance, RSC Adv. 5 (2015) 328–337.
[74] Z. Li, X. Lai, H. Wang, D. Mao, C. Xing, D. Wang, General synthesis of homogeneous hollow core-shell ferrite microspheres, J. Phys. Chem. 113 (2009) 2792–2797.
[75] J.-K. Choi, I.-S. Hwang, S.-J. Kim, J.-S. Park, S.-S. Park, U. Jeong, Y.C. Kang, J.-H. Lee, Design of selective gas sensors using electrospun Pd-doped SnO_2 hollow nanofibers, Sens. Actuators B-Chem. 150 (2010) 191–199.
[76] Y. Li, F. Li, C. Li, W. Wei, D. Jiang, L. Zhu, et al., The preparation of Cr_2O_3@WO_3 hierarchical nanostructures and their application in the detection of volatile organic compounds (VOCs), RSC Adv. 5 (2015) 61528–61534.
[77] S.J. Ippolito, S. Kandasamy, K. Kalantar-zadeh, W. Wlodarski, Hydrogen sensing characteristics of WO_3 thin film conductometric sensors activated by Pt and Au catalysts, Sens. Actuators B-Chem. 108 (2005) 154–158.
[78] M. Hubner, D. Koziej, J.D. Grunwaldt, U. Weimar, N. Barsan, An Au clusters related spill-over sensitization mechanism in SnO_2-based gas sensors identified by operando HERFD-XAS, work function changes, DC resistance and catalytic conversion studies, Phys. Chem. Chem. Phys. 14 (2012) 13249–13254.
[79] H. Zhang, S. Wang, Y. Wang, J. Yang, X. Gao, L. Wang, TiO_2(B) nanoparticle-functionalized WO_3 nanorods with enhanced gas sensing properties, Phys. Chem. Chem. Phys. 16 (2014) 10830–10836.
[80] H. Zhang, R. Wu, Z. Chen, G. Liu, Z. Zhang, Z. Jiao, Self-assembly fabrication of 3D flower-like ZnO hierarchical nanostructures and their gas sensing properties, CrystEngComm 14 (2012) 1775.
[81] D. Bekermann, A. Gasparotto, D. Barreca, C. Maccato, E. Comini, C. Sada, G. Sberveglieri, A. Devi, R.A. Fischer, Co_3O_4/ZnO nanocomposites: from plasma synthesis to gas sensing applications, ACS Appl. Mater. Interface 4 (2012) 928–934.

Biographies

Feng Li is an undergraduate in College of Electronic Science and Engineering, Jilin University, China, and interested in nanomaterials and chemical sensors.

Sijia Guo is an undergraduate in College of Electronic Science and Engineering, Jilin University, China, and interested in nanomaterials and chemical sensors.

Jingli Shen is an undergraduate in College of Electronic Science and Engineering, Jilin University, China, and interested in functional nanomaterials, chemical sensors.

Liang Shen received the PhD degree of electronic science and engineering from Jilin University, China in 2009. Now, he is an associate professor in College of Electronics Science and Engineering, Jilin University, and mainly devoted to the research of polymeric solar cell.

Dongming Sun received the PhD degree from College of Electronics Science and Engineering, Jilin University in 2006. Now he is an associate researcher and mainly devotes to the research of electronic functional materials and devices.

Bin Wang is an undergraduate in national key laboratory, and interested in electronic functional materials and chemical sensors.

Yu Chen received the PhD degree from Institute of Semiconductors, Chinese Academy of Sciences in 2007. Now he is an associate researcher fellow and mainly devotes to the research of material synthesis and electronic functional materials.

Shengping Ruan received the PhD degree of electronic science and engineering from Jilin University in 2001. Now, he is a full professor in the College of Electronics Science and Engineering, Jilin University, and mainly devoted to the research of electronic functional materials and devices.